# Gravity's Action on Light

*A. O. Petters*

*In memory of Vladimir Arnold and David Blackwell*

Gravitational lensing is the action of gravity on light. The subject has become a vibrant area in astronomy and mathematical physics with great predictive power. The field cuts across geometry, topology, probability, and singularity theory and interconnects mathematics, physics, and astrophysics.

The first part of this article gives an introduction to the subject with a review of standard results. The rest of the paper brings the reader to the mathematical forefront of the subject with a treatment of some recent research findings and unsolved problems. In addition, the interdisciplinary features of gravitational lensing are highlighted through the following topics: stability and genericity in lens systems, deterministic and stochastic aspects of image counting, local and global geometry of caustics and cosmic shadow patterns, and magnification relations for stable caustics. We add that the article on lensing by Khavinson and Neumann [40] in the June/July 2008 *Notices* complements this one and was focused primarily on the link between the maximum number of zeros of complex rational harmonic functions and the gravitational lensing problem of the maximum number of lensed images.

Our story begins with Einstein.

*Arlie Petters (AP) is professor of mathematics, physics, and business administration at Duke University. His email address is* arlie.petters@duke.edu. *He is thankful to Amir Aazami, Charles Keeton, Alberto Teguia, and Marcus Werner for constructive feedback on the article and acknowledges partial support from NSF grant DMS-0707003 and hospitality at the Petters Research Institute, where part of this work was done.*

## Einstein and Gravitational Lensing

Even before completing his general theory of relativity, Einstein [25] had explored by 1911 how strongly gravity would bend light grazing a celestial body and implored astronomers to search the heavens for this effect: "It would be highly desirable that astronomers take up the question raised here, even if the considerations should seem to be insufficiently founded or entirely speculative."

It was not until the completion of general relativity in 1915 that Einstein obtained the correct formula for light's bending angle by a static spherically symmetric compact body of mass $\mathsf{m}$:

$$\hat{\alpha}(r) \approx 4\,\frac{\mathsf{m}_\bullet}{r}, \tag{1}$$

where $\mathsf{m}_\bullet = G\mathsf{m}/c^2$ (gravitational radius of lens) with $G$ the universal gravitational constant, $c$ the speed of light, and $r$ the distance of closest approach of the light ray to the center of the lens.

Today we know that Einstein's approximate bending angle formula (1) is the first term in a series (Keeton and AP 2005 [36]):

$$\hat{\alpha}(b) = A_1\left(\frac{\mathsf{m}_\bullet}{b}\right) + A_2\left(\frac{\mathsf{m}_\bullet}{b}\right)^2 + A_3\left(\frac{\mathsf{m}_\bullet}{b}\right)^3 + A_4\left(\frac{\mathsf{m}_\bullet}{b}\right)^4 + A_5\left(\frac{\mathsf{m}_\bullet}{b}\right)^5 + \mathcal{O}\left(\frac{\mathsf{m}_\bullet}{b}\right)^6, \tag{2}$$

where $b$ is called the *impact parameter* and $A_1 = 4$, $A_2 = 15\pi/4$, $A_3 = 128/3$, $A_4 = 3465\pi/64$, and $A_5 = 3584/5$. The distance $r$ of closest approach in (1) is coordinate dependent, whereas the quantities $b$ and $\mathsf{m}_\bullet$ are coordinate independent. Consequently, the series (2) is coordinate independent.

The 1919 observational confirmation of the light bending angle equation (1) for the case of

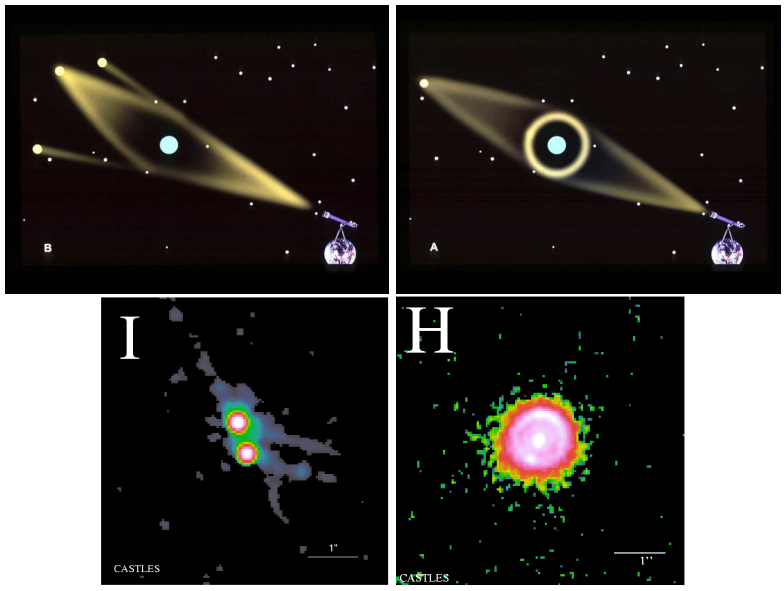


**Figure 1. Top row: Einstein predicted that double images (left panel, outer bright spots) will occur if the light source (bright spot between the outer two) is off the line of sight and lensed by an intermediate compact body (large blue spot). He also argued that if the source is on the line of sight, the source will appear as a bright ring, known today as an *Einstein ring* (right panel). Bottom row: An observed example of double-lensed images (left panel) and an Einstein ring image (right panel) of lensed quasars. The "I" and "H" refer to the infrared wavelength bands used for the observations. Credits: Schoendorf (*Duke Magazine*) and CASTLES [18].**

lensing by the sun gave observational support to Einstein's gravitational theory over Newtonian gravity. It made Einstein a household name and marked the first observation of gravitational lensing. Einstein also discovered two remarkable lensing properties, which he published in 1936 in a short *Science* article [26]. He showed that *double images* can occur when a background light source is off the line of sight. When the source is on the line of sight, a highly magnified ring-like image, now called an *Einstein ring*, can form; see Figure 1.

Einstein was very skeptical that these effects would be observed and, upon the urging of the Czech engineer Rudi Mandl, he reluctantly published the article [54, p. 7]. Fortunately, the advancement of technology over the next four decades set the foundation for the first observation in 1979 of double images of a lensed quasar. This serendipitous breakthrough discovery by Walsh, Carswell, and Weymann [72] marked the transformation of gravitational lensing from an arena of purely theoretical speculation to a data-driven science!

Today, observations of gravitational lensing signatures in the universe abound. Earth- and space-borne telescopes have found multiple images, rings, arcs, and highly magnified images of lensed sources. For lensing by galaxies, data from lens samples like CASTLES [18], SQLS [70], and SLACS [69] reveal scores of examples of multiply imaged quasars and observed ring/arc systems.

## Gravitational Lensing Framework

### The Space-Time Geometry

The light rays in gravitational lensing are modeled by null geodesics that ride the geometry of space-time. The Einstein equation is the physical law governing the interplay between the space-time's geometry and its mass-energy content (lenses). Lensing effects arise when multiple light rays have different arrival times at a given spatial location, light rays converge to create caustics, infinitesimal bundles of light rays experience expansion and/or contraction due to the Ricci curvature and shearing due to the Weyl tensor, etc. These effects are far too complicated to address here in a general space-time framework; see Perlick [48]. We restrict ourselves to the space-time setting relevant to astronomical observations.

Most gravitational lenses can be modeled using the *static*, *thin-lens*, *weak-deflection* approximation, because the observer-lens distance[1] $d_L$ and lens-light source distance $d_{L,S}$ are significantly larger than the diameter of the lens and because the bending angles are much less than unity (e.g.,

[1] *The issue of distance in cosmology is a story unto itself. In fact, the distances in gravitational lensing are typically angular diameter distances; see [66, Sec. 4.5] for details.*

less than an arcminute) [54]. Examples of such lenses are planets, stars like our Sun, and galaxies. This approximation fails for lensing near a black hole because bending angles can exceed 360 degrees! Amazingly, however, the static, thin-lens, weak-deflection approximation is unmatched in the power of its predictions that are accessible to current and near-future instrumentation.

Figure 2 illustrates the above approximation, where $L$ is the lens plane and $S = \mathbb{R}^2$ is the light source plane. The (scaled) positions $\mathbf{x}$ and $\mathbf{y}$ in the figure are given by $\mathbf{x} = \mathbf{r}/d_L$ and $\mathbf{y} = \mathbf{s}/d_S$, where $\mathbf{r}$ is the vector of impact of the light ray in the lens plane, $\mathbf{s}$ is the position of the light source on the light source plane $S$, and $d_L$ and $d_S$ are the respective distances from the observer to $L$ and $S$. Note that $d_S > d_L \gg |\mathbf{r}|$ in a typical astrophysical setting.

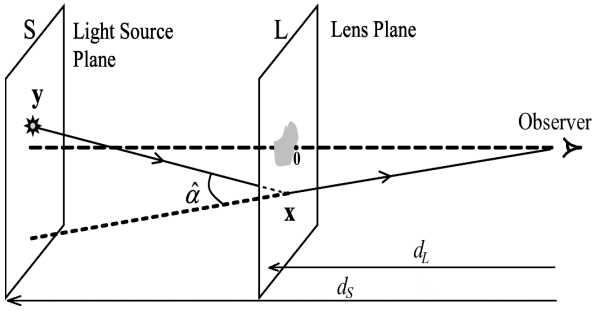


**Figure 2. Schematic of thin-lens, weak-deflection single plane gravitational lensing. The dashed line through the origin is the optical axis of the lens system.**

The space-time geometry for a static,[2] thin-lens, weak-deflection lens has a metric of the form:

$$\mathbf{g}_{\text{weak}} = -\left(1 + \frac{2\phi}{c^2}\right) dt^2 + a^2(t)\left(1 - \frac{2\phi}{c^2}\right) \mathbf{g}_{\text{Euc}},$$

where $|\phi|/c^2 \ll 1$. Here $t = c\tau$, with $c$ the speed of light and $\tau$ cosmological time. The function $a(t)$ accounts for the expansion of the universe. The metric $\mathbf{g}_{\text{Euc}}$ is the standard Euclidean metric on $\mathbb{R}^3$ and $\phi$ is the time-independent, three-dimensional Newtonian potential of the lens with corresponding mass density concentrated about the lens plane. In astrophysical applications, the metric $\mathbf{g}_{\text{weak}}$ is computed only to first order in $\phi/c^2$.

[2] *The static condition means that physically the lens has negligible change over the time interval during which the lensing effect is being observed.*

**Deflection Potential**

In physical modeling of the lens system in Figure 2, the three-dimensional Newtonian potential $\phi$ of the lens is "projected" into the lens plane $L$, creating a two-dimensional Newtonian potential $\psi$ of the lens in $L$ (since the lens is thin and bending angles are small); see [66, Chap. 4] for details. The projected potential $\psi$ is called the *deflection potential* and defined by:

$$\psi(\mathbf{x}) = \frac{2d_{LS}}{c^2 d_L d_S} \int_{\zeta_0}^{\zeta_s} \phi(d_L\mathbf{x}, \zeta)\, d\zeta,$$

where $(\mathbf{x}, \zeta)$ are rectangular coordinates covering the region of space containing the lens system, the $\zeta$-axis coincides with the optical axis of the lens system, and $\zeta_0$, $\zeta_s$ are the respective $\zeta$-locations of the observer and light source plane.

Lensing by $\psi$ produces a weak-deflection bending angle generalizing Einstein's bending angle (1) or, equivalently, the first term in (2), to:

$$\hat{\boldsymbol{\alpha}}(d_L\mathbf{x}) = \frac{d_S}{d_{L,S}} \nabla\psi(\mathbf{x}),$$

where the gradient operator $\nabla$ is relative to rectangular coordinates $\mathbf{x} = (u, v)$ on the lens plane. The physical bending angle is $\hat{\alpha} = |\hat{\boldsymbol{\alpha}}|$. Note that a point mass deflection potential, namely, $\psi(\mathbf{x}) = m \log|\mathbf{x}|$ with $m = 4(d_{L,S}/c^2 d_S)\mathtt{m}$, produces Einstein's bending angle (1).

More formally, the deflection potential is a smooth function $\psi : L \longrightarrow \mathbb{R}$, where $L = \mathbb{R}^2 - A$ models the lens plane, with $A$ a finite set of points representing possible singularities in the lens. The surface mass density $\kappa$ due to $\psi$ is determined by the two-dimensional Poisson equation:

$$\kappa(\mathbf{x}) = \frac{1}{2}\nabla^2\psi(\mathbf{x}),$$

which is the Einstein equation in the present two-dimensional context. The density $\kappa$ causes the expansion or contraction of cross-sections of infinitesimal light ray bundles. Similarly, the gravitational tug due to matter produces shearing across such bundles. The *shear* due to $\psi$ is a rank two symmetric trace-free tensor in $L$, whose independent components $(\Gamma_1(\mathbf{x}), \Gamma_2(\mathbf{x}))$ are defined by:

$$\Gamma_1(\mathbf{x}) = \frac{1}{2}\left[\psi_{uu}(\mathbf{x}) - \psi_{vv}(\mathbf{x})\right], \quad \Gamma_2(\mathbf{x}) = \psi_{uv}(\mathbf{x}).$$

The subscripts indicate partial derivatives relative to (u, v). The *magnitude* of the shear tensor is defined as $\Gamma = \sqrt{\Gamma_1^2 + \Gamma_2^2}$.

**Example: Microlensing Potential.** This lens models a local region of a galaxy lens using three physical components: (1) a collection of $g$ stars with masses $m_1, \ldots, m_g$ at respective positions $\boldsymbol{\xi}_1, \ldots, \boldsymbol{\xi}_g$, (2) a continuous matter component with constant density $\kappa_c \geq 0$ from dark matter, and

(3) a constant shear $\gamma \geq 0$ from the overall gravitational pull of the rest of the galaxy across the local region. The deflection potential and surface mass density of the lens are given respectively by:

$$\psi_g(\mathbf{x}) = \frac{\kappa_c}{2}|\mathbf{x}|^2 - \frac{\gamma}{2}(u^2 - v^2) + \sum_{j=1}^{g} m_j \log|\mathbf{x} - \boldsymbol{\xi}_j|$$

and

$$\kappa_g(\mathbf{x}) = \pi\left(m_1\delta_{\boldsymbol{\xi}_1}(\mathbf{x}) + \cdots + m_g\delta_{\boldsymbol{\xi}_g}(\mathbf{x})\right) + \kappa_c,$$

where $\delta_{\boldsymbol{\xi}_j}(\mathbf{x})$ is the Dirac delta centered at $\boldsymbol{\xi}_j$. The set of singularities of $\psi_g$ is $A = \{\boldsymbol{\xi}_1, \ldots, \boldsymbol{\xi}_g\}$. The $\gamma$ term contributes to the deflection potential $\psi_g$ through a harmonic function and, hence, does not appear in the expression for $\kappa_g$. Also, the magnitude $\Gamma_g$ of the shear tensor converges to the shear from infinity $\gamma$ as $|\mathbf{x}| \to \infty$. The deflection potential $\psi_g$ typically generates lensed images with angular separations of approximately a micro-arcsecond. For this reason, lensing by $\psi_g$ is called *microlensing*.

### Time-Delay Function

The deflection potential $\psi$ induces a family of functions $T : L \times S \to \mathbb{R}$, called a *time-delay family*, defined by:

$$T(\mathbf{x}, \mathbf{y}) = \frac{|\mathbf{x} - \mathbf{y}|^2}{2} - \psi(\mathbf{x}),$$

where $S = \mathbb{R}^2$ is the light source plane (Figure 2) and $\mathbf{y} \in S$. Each function $T_\mathbf{y} : L \to \mathbb{R}$ $T_\mathbf{y}(\mathbf{x}) = T(\mathbf{x}, \mathbf{y})$ in the family $T$ is called a *time-delay function at* $\mathbf{y}$. Physically, the value $T_\mathbf{y}(\mathbf{x})$ is proportional to the arrival time difference measured by the observer between a deflected ray traveling from $\mathbf{y}$ to the observer with impact vector $\mathbf{x}$ and a ray traveling from $\mathbf{y}$ to the observer in the absence of lensing. The arrival time of the unlensed ray enters the time-delay function as a constant and is used simply for convenience. Adding a constant to $T_\mathbf{y}(\mathbf{x})$ has no impact on lensing observables, since they arise from either differences of the time-delay function at lensed images or partial derivatives of the time-delay function [54, Sec. 3.4].

By Fermat's principle [54, p. 66], the light rays connecting $\mathbf{y}$ to the observer have impact vectors given by the critical points[3] of $T_\mathbf{y}$, i.e., solutions $\mathbf{x}$ in $L$ of

$$\nabla T_\mathbf{y}(\mathbf{x}) = \mathbf{0}, \tag{3}$$

where $\nabla$ is relative to the $\mathbf{x}$ coordinates. The light rays will correspond generically to either minima, maxima, or saddles of the time-delay function.

[3] *Generally, we define a* critical point *of a smooth map $f$ from an $n$-manifold $\mathcal{N}$ to an $m$-manifold $\mathcal{M}$ to be a point $x \in \mathcal{N}$, where* $\operatorname{rank}[d_x f] < \min\{n, m\}$.

### Lensing Map and Lensed Images

Every time-delay family $T$ induces a transformation $\boldsymbol{\eta} : L \longrightarrow S$, called a *lensing map*, as follows:

$$\boldsymbol{\eta}(\mathbf{x}) = \nabla T_\mathbf{y}(\mathbf{x}) + \mathbf{y} = \mathbf{x} - \nabla\psi(\mathbf{x}),$$

where $\nabla$ is the $\mathbf{x}$-gradient. A light ray from $\mathbf{y}$ to the observer is then characterized by a solution $\mathbf{x}$ in $L$ of the *lens equation*

$$\boldsymbol{\eta}(\mathbf{x}) = \mathbf{y}. \tag{4}$$

The action of $\boldsymbol{\eta}$ has a simple intuitive interpretation via its lens equation. Reverse the light ray in Figure 2 and imagine the light ray being shot like a cannon ball from the observer to the lens plane. The ray impacts the lens plane at $\mathbf{x}$ and gets deflected at $\mathbf{x}$ by the gravity of the matter lens there, causing the ray to hit the light source plane at $\mathbf{y}$.

The *lensed images* of a light source at $\mathbf{y}$ are then defined to be elements of the fiber $\boldsymbol{\eta}^{-1}(\mathbf{y})$. By the bijection between solutions of (3) and (4), we can naturally identify each lensed image of $\mathbf{y}$ with its associated critical point of $T_\mathbf{y}$. Consequently, when $T_\mathbf{y}$ is nondegenerate, we can assign a Morse index $i_\mathbf{x}$ to a lensed image $\mathbf{x}$ of $\mathbf{y}$, namely, $i_\mathbf{x} = 0$, 1, and 2, respectively, for $\mathbf{x}$ a minimum, saddle, and maximum lensed image. The *parity* of a lensed image $\mathbf{x}$ is defined as the evenness or oddness of $i_\mathbf{x}$ for nondegenerate $T_\mathbf{y}$. A *positive parity* (respectively, *negative parity*) lensed image is one with an even (respectively, odd) parity. The lensed images in Figure 2 form a positive-negative parity pair; one is a minimum lensed image and the other a saddle.

### Magnification of Lensed Images

The *magnification* $M_\mathbf{y}(\mathbf{x})$ of a lensed image $\mathbf{x}$ of a light source at $\mathbf{y}$ is given physically as the ratio of the flux of the image to the flux of the light source in the absence of lensing. It can be shown that:

$$M_\mathbf{y}(\mathbf{x}) = \frac{1}{|\det[\operatorname{Jac}\boldsymbol{\eta}](\mathbf{x})|}, \qquad \boldsymbol{\eta}(\mathbf{x}) = \mathbf{y}.$$

Magnification is a geometric invariant because $M_\mathbf{y}(\mathbf{x})$ is the reciprocal of the Gaussian curvature at the critical point $(\mathbf{x}, T_\mathbf{y}(\mathbf{x}))$ in the graph of $T_\mathbf{y}$. A lensed image $\mathbf{x}$ of $\mathbf{y}$ is *magnified* if $M_\mathbf{y}(\mathbf{x}) > 1$ and *demagnified* when $M_\mathbf{y}(\mathbf{x}) < 1$. The *signed magnification* of a lensed image $\mathbf{x}$ of $\mathbf{y}$ is $\mu_\mathbf{y}(\mathbf{x}) = (-1)^{i_\mathbf{x}} M_\mathbf{y}(\mathbf{x})$, where $\boldsymbol{\eta}(\mathbf{x}) = \mathbf{y}$ and $i_\mathbf{x}$ is the Morse index of $\mathbf{x}$. The *total magnification* of a light source at $\mathbf{y}$ is

$$M_{\text{tot}}(\mathbf{y}) = \sum_{\mathbf{x} \in \boldsymbol{\eta}^{-1}(\mathbf{y})} M_\mathbf{y}(\mathbf{x}).$$

The critical point type of a lensed image has physical relevance. *Minimum lensed images are never demagnified* (Schneider 1984 [64]) and, in fact, are typically magnified in real systems [66, 54]. A minimum lensed image $\mathbf{x}_{\min}$ cannot have an

arbitrary position relative to the lens but is always located where the lens's surface mass density $\kappa$ is subcritical, $0 \le \kappa(\mathbf{x}_{\min}) < 1$, and its magnitude of shear is not supercritical, $0 \le \Gamma(\mathbf{x}_{\min}) \le 1$.

A maximum lensed image $\mathbf{x}_{\max}$ is situated where the surface mass density of the lens is supercritical, $\kappa(\mathbf{x}_{\max}) > 1$. For example, a maximum lensed image produced by a galaxy lens would be located near the dense nucleus of the galaxy, causing the image to be highly demagnified, hence difficult to observe.

No restrictions are known for the positions of saddle lensed images due to general lenses. However, computer simulations of microlensing show that saddle lensed images have a tendency to congregate near the positions of point masses; see [54, Sec. 11.6] for a mathematical result on the trajectories of saddle lensed images.

### Critical Curves and Caustics

The set of *critical points* of $\boldsymbol{\eta}$ is the locus of all $\mathbf{x}$ in $L$ where $\det[\mathrm{Jac}\,\boldsymbol{\eta}](\mathbf{x}) = 0$. This corresponds to the set of all formally infinitely magnified lensed images of all light source positions in the light source plane $S$. A curve of critical points is called a *critical curve* of $\boldsymbol{\eta}$. The set of *caustics* of $\boldsymbol{\eta}$ is the set of critical values of $\boldsymbol{\eta}$, which is the set of all light source positions giving rise to at least one infinitely magnified lensed image. The set of caustics of $\boldsymbol{\eta}$ has measure zero. For a point mass lens, which Einstein studied in 1936 [26], the set of critical points forms a circle called an *Einstein ring*, and the set of caustics is a single point; see Figure 1.

### Multiplane Lensing Framework

The single-plane lensing extends naturally to $k$ lens planes as depicted in Figure 3.

Let $\psi_i : L_i \longrightarrow \mathbb{R}$ be the deflection potential on the $i$th lens plane $L_i$, set $L_{(k)} = L_1 \times \cdots \times L_k$, and let $\mathbf{x}_{k+1} = \mathbf{y}$. A *k-plane time-delay family* induced

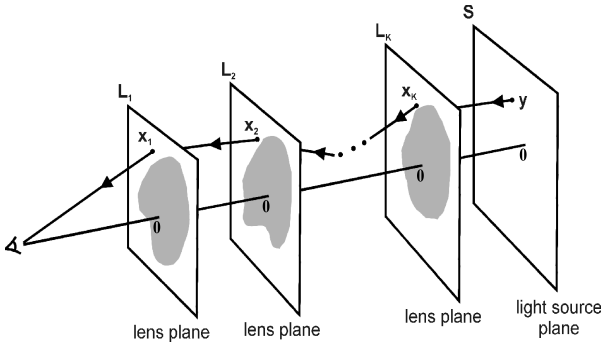


**Figure 3. A schematic of multiplane lensing in the static, thin-lens, weak-deflection approximation. Credits: [54, p. 196].**

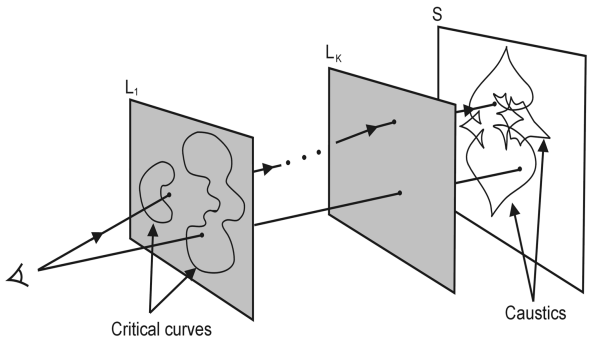


**Figure 4. Critical curves and caustics in multiplane lensing. Note the cusp points and fold arcs on the caustics. Credits: [54, p. 203].**

by these deflection potentials is the function $T_{(k)} : L_{(k)} \times S \longrightarrow \mathbb{R}$ defined by

$$T_{(k)}(\mathbf{x}_1, \ldots, \mathbf{x}_k, \mathbf{y}) = \sum_{i=1}^{k} \vartheta_i \left[ \frac{|\mathbf{x}_i - \mathbf{x}_{i+1}|^2}{2} - \beta_i \psi_i(\mathbf{x}_i) \right],$$

where $\vartheta_i$ and $\beta_i$ are constants involving physical aspects (e.g., distances) of the lens system. The *k-plane lensing map* generated by $T_{(k)}$ is a map of the form $\boldsymbol{\eta}_{(k)} : P \subseteq L_1 \longrightarrow S$, where $P = \mathbb{R}^2 - B$ with $B$ the set of light ray obstruction points, namely, the set of all points in $\mathbb{R}^2$ through which a backwards traced light ray is obstructed from reaching the light source plane (e.g., if a light ray impacts a star). The notions of lensed image, magnification, critical points, and caustics carry over naturally to the $k$-plane case.

**Remark.** The lensing map $\boldsymbol{\eta}_{(k)}$ is generated by the time-delay family $T_{(k)}$ in a manner similar to how Lagrangian maps are formed from their generating family of functions or catastrophe maps are produced from their generating unfoldings. In fact, the Lagrangian map or catastrophe map induced by $T_{(k)}$ is differentiably equivalent to $\boldsymbol{\eta}_{(k)}$.

### Gravitational Lensing Software

A publicly available extensive lensing software is GRAVLENS, which was developed by Keeton: `http://redfive.rutgers.edu/~keeton/gravlens/`. The software computes positions, magnifications, and time delays of lensed images for both point and extended light sources and for essentially arbitrary mass distributions in the lens. The forthcoming version 2.0 (expected 2010) will do stochastic lensing and $k$-plane lensing.

## Stability and Genericity in Lensing

Often astronomers develop intuition into lensing from the analysis of overly simplified analytical models. There is then a need for general theoretical lensing results that capture the properties of lens systems that are shared by most such systems and that persist even under the many small

perturbations affecting these systems in their cosmic environment. We desire a characterization of the *generic, stable features* of $k$-lens systems that are independent of the specific fine details of the system.

A *generic property* in a space[4] of maps is a property common to all maps in an open dense subset of the space. Of course, a precise definition of stability is beyond the scope of this article, so we shall employ an informal characterization; see [30] and [54, Chap. 7] for rigorous treatments.

Intuitively, a lensing map $\boldsymbol{\eta}_{(k)}$ is "locally stable" if any sufficiently small perturbation $\widehat{\boldsymbol{\eta}_{(k)}}$ of $\boldsymbol{\eta}_{(k)}$ (not necessarily a linear perturbation) has the same local critical point structure as $\boldsymbol{\eta}_{(k)}$ up to a coordinate change. It can be shown that a lensing map $\boldsymbol{\eta}_{(k)}$ is *locally stable* if and only if its caustics are locally either fold arcs or cusp points. In this case, the set of critical points form disjoint nonself-intersecting curves (critical curves), whose total number we can bound in some cases (e.g., Theorem 8). Note that the lensing map of a point mass lens, which was studied by Einstein in 1936 [26], is not locally stable because the caustic is a point, though the critical curve is a circle; see Figure 1.

A lensing map $\boldsymbol{\eta}_{(k)}$ is *transverse stable* if and only if $\boldsymbol{\eta}_{(k)}$ is locally stable and its caustics curves are "stably distributed", namely, each intersection of fold arcs occurs at a nonzero angle, no more than two fold arcs cross at the same point, no fold arc passes through a cusp point, and no two cusp points coincide.

The theorem below, which was established in the monograph [54] by AP, Levine, and Wambsganss, characterizes the generic properties of $k$-plane lens systems:

**Theorem 1.** [54, p. 311] *Let $\mathfrak{T}_{(k)}$ be the space of all $k$-plane time-delay families $T_{(k)} : L_{(k)} \times S \longrightarrow \mathbb{R}$ and let $\mathfrak{T}^{\star}_{(k)}$ be the subset of $\mathfrak{T}_{(k)}$ of all $k$-plane time-delay families whose lensing maps are transverse stable. Then $\mathfrak{T}^{\star}_{(k)}$ is open and dense in $\mathfrak{T}_{(k)}$.*

A sketch of the proof of Theorem 1 is beyond the scope of this article. It utilizes the technical machinery of multijet transversality to singularity manifolds. Theorem 1 implies that among the vast array of gravitational lens systems in the cosmos that fall within the static, thin-lens, weak-deflection approximation, the associated lensing map is typically transverse stable. In addition, for a dense subset of light source positions, the corresponding lensed images are either minima, maxima, or generalized saddles, no matter how complex the lens system; see [54, Chap. 8].

[4] *We assume that a space of maps between smooth manifolds has the Whitney $C^{\infty}$ topology.*

## Image Counting

As early as 1912 [61], Einstein had found that a lens consisting of a single star (point mass) will produce *two* lensed images of a background star that is not on a caustic. For two point masses on the same lens plane, Schneider and Weiss 1986 [67] employed lengthy, intricate calculations to show that this lens produces *three* or *five* lensed images of a light source not on a caustic. Naturally, one would like to know how many lensed images are produced by $g$ stars or, generally, by a generic gravitational lens system.

In 1991 AP [49] addressed the image counting problem using *Morse theory under boundary conditions A and B* to obtain counting formulas and a minimum for the total number of images due to a generic $k$-plane gravitational lens system. An added benefit from the Morse theoretic approach is that it applies to generic $k$-plane lensing and generalizes naturally to Lorentzian manifolds; see Perlick [48] and references therein.

For simplicity, we present a sample of image counting results due only to lensing by point masses (stars).

**Theorem 2.** [49] *If a light source, not on a caustic, undergoes single-plane lensing by $g$ point masses, then:*

(1) *There are no maximum lensed images.*
(2) *The total number $N$ of lensed images obeys:*

$$N = 2N_{\min} + g - 1 = 2N_{\text{sad}} - g + 1,$$

*where $N_{\min}$ and $N_{\text{sad}}$ are the number of minimum and saddle lensed images, respectively.*
(3) *The minimum value of $N$ is $g + 1$.*

The counting formula in Theorem 2 is useful for checking whether software that numerically searches the lens equation for microimages has overlooked some—e.g., a system with 10,000 stars has more than that many microimages. The counting formula also shows that the total number of lensed images is even (odd) if and only if the number of point masses is odd (even).

For the maximum number of lensed images, Rhie 2003 [62] constructed an example of lensing by $g$ point masses that produce $5g - 5$ lensed images for $g \geq 2$, which she conjectured is the maximum possible; see [57] for a brief history. Khavinson and Neumann 2006 [39] settled the conjecture by translating the problem into determining the maximum number of zeros of a complex rational harmonic function of the form $r(z) - \bar{z}$, where $r(z) = p(z)/q(z)$ with $p(z)$ and $q(z)$ relatively prime polynomials and $\deg r = \max\{\deg p, \deg q\} = g$. We note that Kuznia and Lundberg 2009 [41] studied the case where $r(z)$ is a Blaschke product and found a maximum of $g + 3$ zeros.

**Theorem 3.** [62, 39] *A light source, not on a caustic, that is lensed by $g$ point masses on a single lens plane has a maximum number of lensed images of $5g-5$ for $g \geq 2$.*

By Theorems 2 and 3, we have $g+1 \leq N \leq 5g-5$ for $g \geq 2$, which yields that two point masses will produce three, four, or five lensed images. But $N$ has parity (evenness or oddness) opposite to $g$, so four images cannot be produced. Hence, we immediately recover the result in [67] that two stars produce three or five images of a light source not on a caustic.

The multiplane analogue of Theorem 2 is:

**Theorem 4.** [49, 51] *If a light source, not on a caustic, undergoes $k$-plane lensing by point masses with $g_i$ point masses on the $i$th lens plane, then:*

(1) *There are no maximum lensed images.*

(2) *The total number $N$ of lensed images obeys:*

$$N = 2N_+ - \prod_{i=1}^{k}(1-g_i) = 2N_- + \prod_{i=1}^{k}(1-g_i),$$

*where $N_\pm$ is the number of even/odd index lensed images.*

(3) *The minimum value of $N$ is $\prod_{i=1}^{k}(g_i+1)$.*

Theorem 4 immediately shows that if any lens plane has only one point mass, then the total number of lensed images is always *even*. This is complemented by the fact that there is an *odd number of lensed images due to $k$-plane lensing by nonsingular lenses* [49, 51].

No multiplane analogue of Theorem 3 exists as of the writing of this article. However, an upper bound was found by AP [53] in 1997 using a resultant approach:

**Theorem 5.** [53] *If a light source, not on a caustic, is lensed by $g$ point masses distributed in space with one point mass on each lens plane, then the number of images is bounded as follows:*

$$2^g \leq N \leq 2\left(2^{2(g-1)}-1\right),$$

*where the lower bound is sharp (attainable).*

The sharp lower bound in Theorem 5 follows from Theorem 4(3) since $g_i = 1$ for $i = 1, \ldots, g$.

**Open Problem 1.** Determine the maximum number of lensed images due to $g$ point masses distributed in space with one point mass on each lens plane.

There is no global maximum number of lensed images due to lensing by general nonsingular gravitational lenses. This is because one can always add an appropriate smooth mass clump to a nonsingular lens to produce extra images. Note that a global minimum exists for the number of lensed images due to multiplane singular lenses with time-delay functions satisfying Morse boundary conditions A. In fact, the global minimum is also given by Theorem 4(3) [51].

A maximum number of lensed images due to nonsingular lenses can be found in certain special cases. For example, in 2007 Fassnacht, Keeton, and Khavinson proved that an elliptical uniform mass distribution produces a maximum of four images external to the lens [29]. Khavinson and Lundberg 2010 [37] showed that multiple imaging by finitely many disjoint radially symmetric disc lenses is more complex than was originally thought by constructing an example with five such lenses that surprisingly produces twenty-seven lensed images, where twenty-five images would have been expected. Khavinson and Lundberg 2010 [38] also showed that there are at most eight external lensed images due to an elliptic lens with isothermal density, which was followed by recent work of Bergweiler and Eremenko 2010 [14] proving that the maximum number is actually six. This problem involved studying zeros of complex transcendental harmonic functions as opposed to the complex rational harmonic functions found in microlensing.

**Open Problem 2.** Determine the maximum number of lensed images due to elliptical isothermal lenses distributed over multiple lens planes.

## Stochastic Gravitational Lensing

In lensing we often do not know the positions of stars, the locations of dark matter clumps, etc., and have to treat such components of a lens system as random. For these situations, the induced time-delay family and its lensing map are random and connect naturally with the *geometry of random fields*.

The theory of random fields has been developed largely around the tractable case of Gaussian fields. Interested readers may consult, for example, the seminal works of Adler, Berry, Hannay, Longuet-Higgins, Nye, Taylor, Upstill, Worsham, etc.; see [5], [6], [7], [15]. Interestingly, the key random fields in gravitational lensing are, in general, not Gaussian.

### Non-gaussianity and Stochastic Microlensing

Consider a random microlensing deflection potential $\psi_g$ where all the point masses have the same mass $m_i = m$ and their positions $\boldsymbol{\xi}_i$ are *independent and uniformly distributed* in the disc $B(\mathbf{0}, R)$ of radius $R = \sqrt{g/\pi}$ centered at the origin of the lens plane. Let $T_{\mathbf{y},g}$, $\boldsymbol{\eta}_g$, and $\mathbf{G}_g = (\Gamma_{1,g}, \Gamma_{2,g})$ be, respectively, the single-plane time-delay function, lensing map, and pair of shear tensor components due to the given $\psi_g$. Set $T^*_{\mathbf{y},g}(\mathbf{x}) = T_{\mathbf{y},g}(\mathbf{x}) + gm\log R$ and $\boldsymbol{\eta}^*_g(\mathbf{x}) = \boldsymbol{\eta}_g(\mathbf{x})/\sqrt{\log g}$. Denote the probability density functions (p.d.f.'s) of $T^*_{\mathbf{y},g}(\mathbf{x})$, $\boldsymbol{\eta}^*_g(\mathbf{x})$, and $\mathbf{G}_g(\mathbf{x})$ by $f_{T^*_{\mathbf{y},g}(\mathbf{x})}$, $f_{\boldsymbol{\eta}^*_g(\mathbf{x})}$, and $f_{\mathbf{G}_g(\mathbf{x})}$, respectively.

AP, Teguia, and Rider 2009 [55, 56] showed:

**Theorem 6.** [55, 56] *For the above random microlensing deflection potential $\psi_g$, the p.d.f.'s $f_{T^*_{\mathbf{y},g}(\mathbf{0})}$, $f_{\boldsymbol{\eta}^*_g(\mathbf{x})}$, and $f_{\mathbf{G}_g(\mathbf{x})}$, where $\mathbf{x} \in B(\mathbf{0},R)$, are* ***not*** *Gaussian for $g = 1,2,\ldots$. As $g \to \infty$, the asymptotic forms are:*

(1) $f_{T^*_{\mathbf{y},g}(\mathbf{x})}(\mathbf{t}) = f_{\mathrm{Gm},g}(\mathbf{t}) + O(1/g^{3/2})$

(2) $f_{\boldsymbol{\eta}^*_g}(\mathbf{k}) = f_{\mathrm{Gs},g}(\mathbf{k})[1 + E_g(\mathbf{k})] + O\left(1/\log g\right)$

(3) $f_{\mathbf{G}_g(\mathbf{x})}(\mathbf{g}) = f_{\mathrm{Ch},g}(\mathbf{g})[1 + H_g(\mathbf{g})] + O\left(1/g^3\right)$,

*where $f_{\mathrm{Gm},g}$, $f_{\mathrm{Gs},g}$, and $f_{\mathrm{Ch},g}$ are gamma, bivariate Gaussian, and stretched bivariate Cauchy densities, respectively. See* [55, 56] *for explicit forms of the integrable functions $E_g$ and $H_g$.*

To illustrate a random $\boldsymbol{\eta}_g$, let $\kappa_c = 0.405$, $\gamma = 0.3$, and $\kappa_* = \pi m = 0.045$. In [55] it was shown that when $g$ is a million, there is a 56% probability that the random lensing map $\boldsymbol{\eta}_g : L \longrightarrow S$ will map a point $\mathbf{x}_0 = (u_0, v_0)$ in $L$ to a point inside a disc of angular radius $r_0 = 0.1$ centered at $\mathbf{a}_0 = ((1 - \kappa_c + \gamma)u_0, (1 - \kappa_c + \gamma)v_0))$. The probability jumps to 97% for mapping $\mathbf{x}_0$ inside a radius $2r_0$ centered at $\mathbf{a}_0$.

### Global Expectation and the Kac-Rice Formula

For a random time-delay function $T_{\mathbf{y}}$, let $N_+(D,\mathbf{y})$ be the random number of positive parity lensed images inside a closed disk $D$ in the lens plane. Under appropriate physically reasonable conditions, the theory of random fields [5, 6] yields that the expectation of $N_+(D,\mathbf{y})$ can be obtained using a Kac-Rice type formula [56]:

$$(5)\quad E[N_+(D,\mathbf{y})] = \int_D E\left[\det[\mathrm{Jac}\,\boldsymbol{\eta}](\mathbf{x})\,\mathbf{1}_{\mathcal{G}_A}(\mathbf{x})\,\middle|\,\boldsymbol{\eta}(\mathbf{x}) = \mathbf{y}\right] f_{\boldsymbol{\eta}(\mathbf{x})}(\mathbf{y})\,\mathrm{d}\mathbf{x},$$

where $\mathbf{1}_{\mathcal{G}_A}$ is the indicator function on

$$\mathcal{G}_A = \{\mathbf{x} \in \mathbb{R}^2 : \det[\mathrm{Jac}\,\boldsymbol{\eta}](\mathbf{x}) \in (0,\infty)\},$$

and $f_{\boldsymbol{\eta}(\mathbf{x})}$ is the p.d.f. of the lensing map at $\mathbf{x}$.

For most applications, equation (5) is insufficient because the light source position $\mathbf{y}$ is not known and so is a random vector. It is physically natural then to generalize (5) by averaging out the light source position. This introduces the notion of "global expectation". Let $\{\mathfrak{F}\}$ be a countable compact covering of $S$ where every $\mathfrak{F}$ has the same positive Lebesgue measure $|\mathfrak{F}_0|$. Construct a family $\{\mathbf{Y}_{\mathfrak{F}}\}$ of random light source positions $\mathbf{Y}$, where $\mathbf{Y}_{\mathfrak{F}}$ is uniformly distributed on $\mathfrak{F}$. The *global expectation* of the number of positive parity lensed images will be denoted by $\widehat{E}[N_+(D,\mathbf{Y};\mathfrak{F})]_{\{\mathfrak{F}\}}$ and defined to be the mean of $E[N_+(D,\mathbf{y})]$ over the family $\{\mathbf{Y}_{\mathfrak{F}}\}$.

AP, Rider, and Teguia 2009 [56] used the Kac-Rice technology to obtain:

**Theorem 7.** [56] *The global expectation of the number of positive parity lensed images in $D$ is:*

$$\widehat{E}[N_+(D,Y;\mathfrak{F})]_{\{\mathfrak{F}\}} = \frac{1}{|\mathfrak{F}_0|}\int_D E\left[\det[\mathrm{Jac}\,\boldsymbol{\eta}](\mathbf{x})\,\mathbf{1}_{\mathcal{G}_A}(\mathbf{x})\right]\,\mathrm{d}\mathbf{x}.$$

Theorem 7 applies to generic lensing scenarios. Furthermore, the theorem is not merely formal because it can be used to calculate the global expected number of minimum lensed images in stochastic microlensing. For example, it was shown in [56] that if $g = 1000$, $\kappa_{\mathrm{tot}} = \kappa_c + \kappa_* = 0.45$, and $(\gamma, \kappa_*)$ varies over the physically reasonable values $(0.n, 0.n)$, where $n = 1,2,3,4$, then the global expected number of minimum microimages is between one and three even though there are over $1,000$ microimages. Hence, there are few minimum lensed images compared to saddles for these parameters. Bear in mind, however, that the global expected mean number of minimum lensed images is divergent for $(1 - \kappa_{\mathrm{tot}})^2 = \gamma^2$.

**Open Problem 3.** Develop a general mathematical theory of stochastic gravitational lensing.

Initial steps were taken in [55, 56] for stochastic microlensing and in [33] for the case of lensing by randomly distributed dark matter clumps in galaxies, but a vast array of statistical and probabilistic issues remain unexplored.

## Caustics

### Counting Caustic Curves and Cusps

For the case of microlensing, some global quantitative results are known about the caustics:

**Theorem 8.** *Consider a locally stable single-plane lensing map due to the microlensing deflection potential $\psi_g$. Then:*

(1) [74] *The number of critical curves is at most $2g$.*

(2) [66, 54] *The number of cusps is even.*

(3) [60] *The number of cusps is bounded above as follows:*

$$0 \le N_{\mathrm{cusps}} \le \begin{cases} 12g^2 & \text{if } \gamma > 0 \\ 12g(g-1) & \text{if } \gamma = 0. \end{cases}$$

(4) [52] *The total signed curvature $K_f$ of the fold caustics satisfies:*

$$K_f = -2\pi g.$$

In Theorem 8, the *even number cusp* and *total signed curvature* results extend to generic $k$-plane lensing (AP 1995 [52]), where for the latter we have

$$K_f = -2\pi|\mathcal{B}|,$$

with $|\mathcal{B}|$ the number of obstruction points in the lens system; also see [54, Sec. 15.4] for more. Figure 5 captures the even-number-cusp result.

**Open Problem 4.** Determine the maximum number of cusps in microlensing.

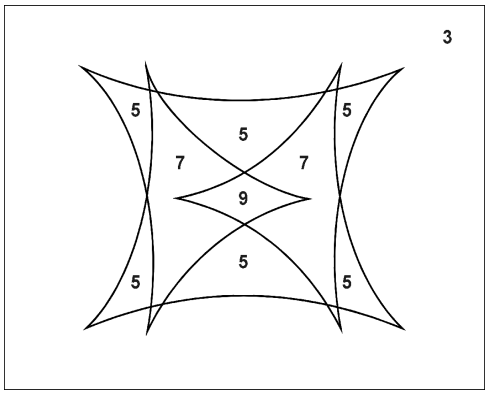


**Figure 5. An illustration of the even-number-cusp theorem and local-convexity theorem. For the latter, fold curves are convex (outward curving) locally on the side from which a light source has more images. Each numeral indicates the number of lensed images of a light source in the given region. These caustics are due to two point mass lens with shear $\gamma > 0$. Credits: [74].**

We suspect that the techniques involved with this problem are similar to the complex algebraic methods employed by Khavinson and Neumann [39] to address the maximum number of lensed images.

### Local Convexity of Caustics

The fold caustic curves due to single-plane lensing by the microlensing deflection potential $\psi_g$ satisfy local convexity, which means that the fold caustic curve is convex (bends outward) when viewed from the side where a light source has more images. This phenomenon was discovered in 1976 by Berry [13] while studying the caustics due to water droplets. The notion was mathematically developed in [54, Sec. 9.3] for the context of gravitational lensing.

**Theorem 9.** [54, p. 360] *If $\boldsymbol{\eta}_p$ is a locally stable single-plane lensing map induced by a deflection potential $\psi$ with a locally constant surface mass density $\kappa$, then the fold arc caustics of $\boldsymbol{\eta}$ are locally convex.*

Theorem 9 applies to the microlensing deflection potential $\psi_g$ since $\kappa_g(\mathbf{x}) = \kappa_c$ for $\mathbf{x} \in L$. Consequently, caustics due to stars cannot bend arbitrarily. Figure 5 gives an example of local convexity in microlensing. Local convexity, however, can be violated for 2-plane lensing by locally constant surface mass densities. For example, 2-plane microlensing can produce teardrop caustics [59].

### Caustic Metamorphoses

For the time-delay families considered so far, all physical parameters of the lens system, such as the masses of the lenses, distances between lens planes, redshifts, etc., are assumed fixed. Allowing these parameters to vary will produce higher order caustic singularities whose contours on the light source plane produce fascinating caustic metamorphoses that can be classified into characteristic types. Note that generic optical caustic metamorphoses have distinct global properties enforced for general caustic metamorphoses—e.g., in three-space, saucer shape or pancake caustics cannot occur in optical caustic metamorphoses (Chekanov 1986 [22]).

Generically, there are five local 1-parameter metamorphoses of caustics in the plane: *lips*, *beak-to-beaks*, *swallowtails*, *elliptic umbilics*, and *hyperbolic umbilics* (Zakalyukin 1984 [75], Arnold 1986 [9], Arnold 1991 [10]). All five of these caustic metamorphoses occur in gravitational lensing [66, 54].

Figure 6 depicts an example of four swallowtail metamorphoses due to lensing by a point mass lens with shear $\gamma = 0.2$ and $\kappa_c = 1.21$. For the general microlensing deflection potential $\psi_g$, only beak-to-beaks, swallowtails, and elliptic umbilics can occur because lips and hyperbolic umbilics violate the local convexity of Theorem 9.

The following results are known about upper bounds on the number of caustic metamorphoses in microlensing:

**Theorem 10.** *Consider a single-plane lensing map due to the microlensing deflection potential $\psi_g$. Then:*

(1) [74] *The number of beak-to-beak caustic metamorphoses is at most $3g - 3$.*
(2) [54, p. 536] *The number of elliptic umbilic caustic metamorphoses is at most $2g-2$ for $\gamma = 0$ and $2g$ for $\gamma > 0$.*

Theorem 10 immediately shows that a single point mass lens with continuous matter and shear cannot produce any beak-to-beak caustic metamorphoses.

**Open Problem 5.** Determine the maximum number of swallowtail metamorphoses in microlensing.

This problem relates to Open Problem 4 since the maximum number of cusps would be an upper bound for the number of swallowtails.

### Elimination of Cusps

Caustic metamorphoses can also eliminate singularities on caustic curves, a result shown for microlensing by AP and Witt in 1996:

**Theorem 11.** [60] *Let $\boldsymbol{\eta}$ be the single-plane lensing map induced by the microlensing deflection potential $\psi_g$. For a sufficiently large continuous dark matter density $\kappa_c$, all the cusp caustics are eliminated, and the caustics evolve into a disjoint collection of $g$ oval, fold caustic curves.*

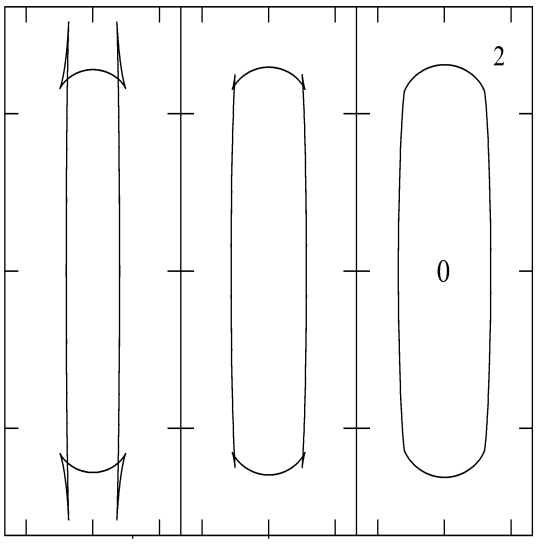


**Figure 6. An illustration of swallowtail metamorphoses and the cusp-elimination theorem (Theorem 11). The left panel shows a caustic with four swallowtail caustic metamorphoses, which yields a total of eight cusps. All the cusps get eliminated by the swallowtail caustic metamorphoses. A light source inside the oval caustic in the right panel will have no lensed images, whereas two lensed images are produced for light source positions outside the oval. Hence, the local-convexity theorem is satisfied by the oval caustic. The caustics are produced by a point mass lens with shear $\gamma = 0.2$ and $\kappa_c$ that increases from left to right through the panels, starting at $\kappa_c = 1.21$ in the left panel. Credits: [54, p. 385].**

Theorem 11 shows that the lower bound on the number of cusps in Theorem 8(3) is not trivial but is the minimum number of cusps. Figure 6 gives an example of cusp elimination leading to an oval caustic. The bottom left panel of Figure 8 also shows some oval caustics.

**Open Problem 6.** Determine whether cusp elimination holds for any locally stable $k$-plane lensing map, where each stage of the evolution is a $k$-plane lensing map.

The notion of cusp elimination for general maps was anticipated by Levine [42] as early as 1963 and further explored by Eliashberg [27] in 1970, giving rise to the Levine-Eliashberg cusp-elimination theorem: A locally stable map from a compact, oriented $n$-manifold into the plane is homotopic to a locally stable map with zero or one cusp if the Euler characteristic of the manifold is even or odd, respectively.

**Remark.** The Levine-Eliashberg cusp-elimination theorem does not imply that cusp elimination holds in gravitational lensing, since if one starts with a lensing map whose domain is extended to the celestial sphere, then the theorem does not guarantee that each stage of the homotopy is a lensing map. Nevertheless, it was this theorem that inspired Theorem 11.

### Arnold's ADE-Family of Caustics

In addition to the light source position $\mathbf{y}$, a lens system has other physical parameters $\mathbf{p} \in \mathbb{R}^{n-2}$, which can represent masses, core radii, shears, redshifts, angular diameter distances, etc. So far, these parameters have been fixed, and only $\mathbf{y}$ was varied.

When we allow the parameters $\mathbf{p}$ to vary as well, we have an $n$-parameter family $T_{\mathbf{p},\mathbf{y}}$ of time-delay functions that generate higher-order caustics in $\mathbb{R}^{n-2} \times S = \{\mathbf{p}, \mathbf{y}\}$. Slices through these higher-dimensional caustics by the light source plane $S$ produce caustic curves in $S$ with distinctive features; see the sketches by Callahan [19].

The local classification of higher-order caustics for general $n$-parameter families is well known from singularity theory (e.g., [8, 11, 12, 21, 54, 46]):

- $n = 2$: *folds* $A_2$ and *cusps* $A_3$.
- $n = 3$: list for $n = 2$ along with *swallowtails* $A_4$, *elliptic umbilics* $D_4^-$, and *hyperbolic umbilics* $D_4^+$.
- $n = 4$: list for $n = 3$ along with *butterflies* $A_5$ and *parabolic umbilics* $D_5$.
- $n = 5$: list for $n = 4$ along with *wigwams* $A_6$, *second elliptic umbilics* $D_6^-$, *second hyperbolic umbilics* $D_6^+$, and *symbolic umbilics* $E_6$.

The $A, D, E$ notation is due to Arnold, who connected these caustic singularities with Coxeter-Dynkin diagrams of simple Lie algebras with the same designation. Arnold's classification of typical caustics for $n \leq 5$ is:

**Theorem 12.** [8] *For $n \leq 5$, there is an open dense set in the space of Lagrangian maps of $n$-dimensional Lagrangian submanifolds such that the caustics of each Lagrangian map in the set are locally from the following list: $A_\ell (1 \leq \ell \leq n+1)$, $D_\ell (4 \leq \ell \leq n+1)$, $E_6 (5 \leq n)$, $E_7 (6 \leq n)$, and $E_8 (7 \leq n)$.*

Figure 7 illustrates the swallowtail $A_4$, elliptic umbilic $D_4^-$, and hyperbolic umbilic $D_4^+$ caustic surfaces from Arnold's ADE-list of caustics in Theorem 12. Generic slices of these caustic surfaces by a plane produce the characteristic shapes of the caustics curves. Note that the figure includes the swallowtail caustic metamorphoses in Figure 6 and three of the five generic local caustic metamorphoses mentioned earlier.

Though Theorem 12 applies to general Lagrangian maps, Guckenheimer [32] showed that it also exhausts the list of typical caustics due to

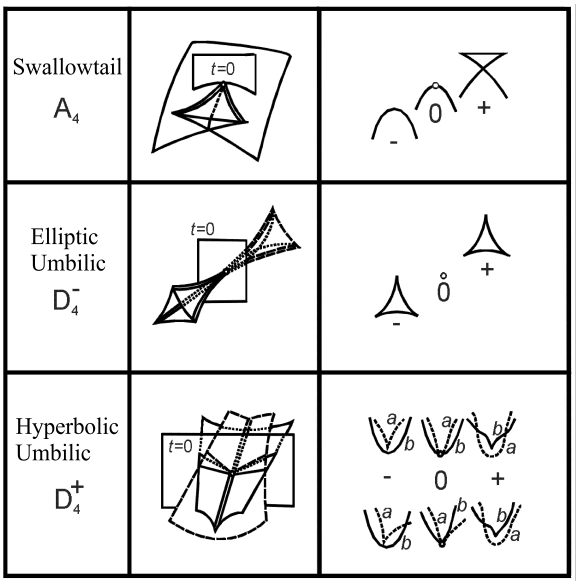


**Figure 7. Swallowtail, elliptic umbilic, and hyperbolic umbilic caustic surfaces. The slices through the caustic surfaces produce planar caustic curves with characteristic features that occur in gravitational lensing. Credits: [9].**

general optical systems. Since gravitational lens systems form a proper subset of the set of optical systems, we need to address whether Arnold's entire ADE-list of caustics occurs in gravitational lensing.

Gravitational lens models are known to produce at least the seven caustics for the $n = 4$ case in Arnold's Theorem 12 [54]. Shin and Evans 2007 [71] showed that our Milky Way galaxy acting as a lens can produce butterfly caustics. Orban de Xivry and Marshall 2009 [47] also developed an atlas of lensing signatures, predicting that a galaxy with a misaligned disc and nucleus would produce swallowtails and butterflies, binary galaxies would generate elliptic umbilics, and clusters of galaxies would produce hyperbolic umbilics and more.

Gravitational lensing by the Abell 1703 cluster of galaxies already reveals a hyperbolic umbilic signature [47]. Current and planned wide-field optical imaging surveys are expected to find thousands of new lensing signatures, which will likely contain evidence for many ADE-caustics [47].

**Remark.** Along with Theorem 12, the wider Arnold singularity theory also applies to gravitational lensing. AP 1993 [50] employed the theory to obtain local classifications of the qualitative features of certain key structures in lensing: *lensed image surfaces* (multibranched graphs of all lensed images with respect to light source position), *multibranched graphs of lensed image time delays*, *Maxwell sets* (light source positions for which at least two lensed images have identical time delays), *bicaustics* (paths traced out by cusps during an evolution of caustics), etc.

## Caustics and Cosmic Shadows

One of the striking consequences of gravitational lensing is that the gravitational fields due to bodies in the universe such as stars, galaxies, black holes, dark matter, etc., cast *shadow patterns* throughout the cosmos. Some examples are shown in Figure 8.

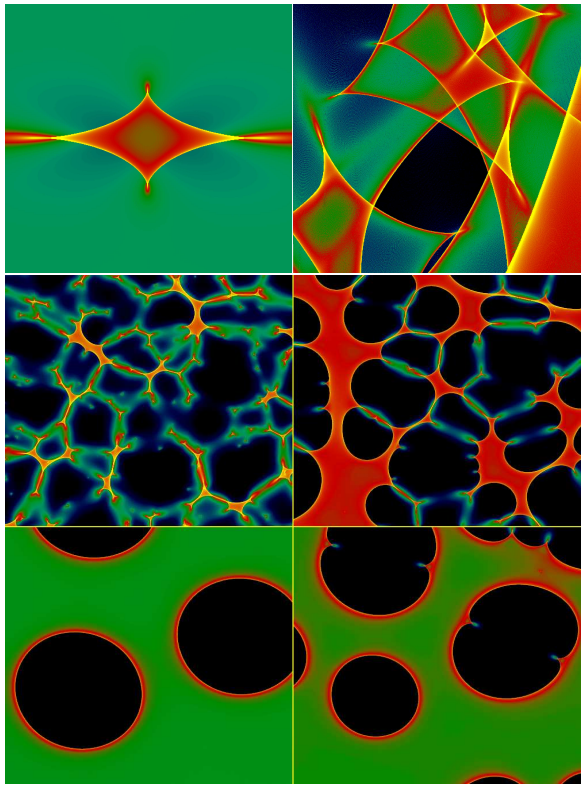

**Figure 8. Examples of shadow patterns on the light source plane generated by microlensing. The fold caustic curves are brighter locally on one side, and each cusp has an emanating bright lobe. Elimination of cusps occurs for the middle and bottom rows of panels (clockwise through those panels), resulting in oval caustics bounding demagnified regions. The shadow pattern color scheme is: yellow (brightest) → red → green → blue → black (darkest). Credits: Wambsganss.**

Within our framework, the shadow pattern lies on the light source plane and is modeled by assigning at each point $\mathbf{y}$ in the light source plane $S$ the total magnification $M_{\text{tot}}(\mathbf{y})$ of a light source at $\mathbf{y}$. As $\mathbf{y}$ varies, a gradation in magnification is mapped out on the light source plane with caustics as the brightest part of the shadow pattern—Figure 8.

Making use of Theorem 1 we can infer the generic properties of the shadow pattern due

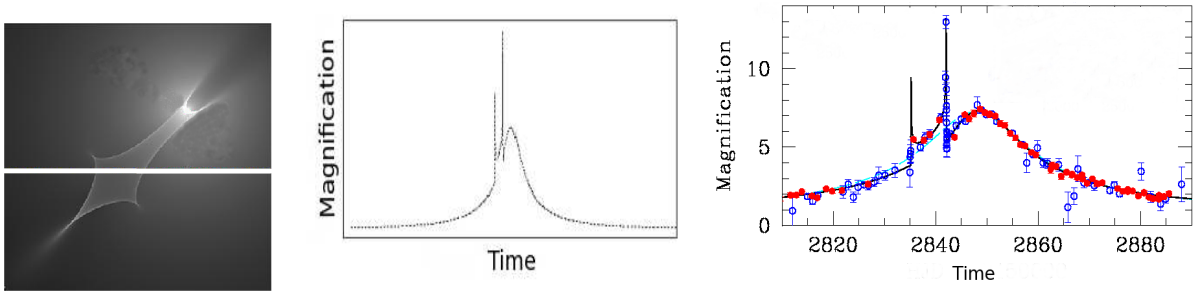


**Figure 9. Finding an extrasolar planet using gravitational lensing. *Leftmost panel:* A theoretical shadow pattern due to a foreground star-planet lens. A background star moves from left to right along the white linear path. *Middle panel:* As the background star cuts through the shadow pattern due to lensing by the foreground star-planet lens (trajectory in the left panel), the background star's magnification varies according to the theoretical light curve shown. The spikes are due to the presence of the planet, which creates the caustic curve shown in the leftmost panel. In the absence of a planet, the light curve would have no spikes and be smooth. *Rightmost panel:* The theoretical light curve in the middle fits observational data of a background star being lensed by a star-planet lens located toward the center of our galaxy. The dots are observations made by the MAO (blue) and OGLE (red) groups. Credits: Bond et al., MAO and OGLE collaborations [17].**

to multiplane lensing. Two such properties are (cf. Figure 8): (1) a fold caustic curve is brighter locally on one side of the curve and (2) cusp caustics, though they form a set of measure zero, contribute nonzero area to a shadow pattern since a high-magnification lobe emanates from each cusp.

## How to Detect an Extrasolar Planet?

The issue of extraterrestrial life has resurged in the media recently with Stephen Hawking's Discovery Channel series. A natural step in the search for life in other parts of our galaxy is to find planets outside our solar system. Gravitational lensing of light sources cutting across shadow patterns provides a powerful tool.

The method is summarized in Figure 9. Suppose that a star and planet lens a background star moving across the line of sight. The star-planet lens creates a shadow pattern on the light source plane (leftmost panel, Figure 9). Note that during the period of observation, the background star typically travels a short distance compared to the scale of the lens system and so its trajectory can be modeled by a linear path.

As the background star cuts across the shadow pattern (leftmost panel, Figure 9), the background star's total magnification will vary according to the brightness gradation in the shadow pattern. The plot of this magnification as a function of position along the linear path is called a *light curve*.

The crossing of caustics by a lensed light source causes significant jumps in the magnification of the source. In the middle panel of Figure 9, the predicted theoretical light curve shows characteristic spikes as the light source crosses the two fold arcs of the caustic. These significant spikes are due to the planet, though the planet is at least a million times less massive than the star. The light curve would be smooth in the absence of the planet [17]. Remarkably, such spikes in light curves have led to the discovery of several extrasolar planets [28].

The alert reader may be disturbed by the shadow pattern in the left panel of Figure 9 due to a star-planet lens. The caustic appears to have five cusps, contradicting the even-number cusp theorem. The issue is resolved in Figure 10.

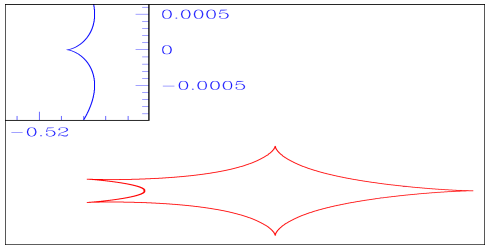


**Figure 10. The caustic in the left panel of Figure 9 appears to have five cusps, violating the even-number cusp theorem. There is actually a hidden extra cusp (insert) on the arc joining the two leftmost cusps. Credits: [54, p. 125].**

## Magnification Relations in Lensing

Qualitative and quantitative results play important roles in gravitational lensing. The former focuses on properties that arise from or are preserved by nonlinear coordinate transformations in the lens and light source planes—e.g., the generic, stable, and topological results of Theorems 1, 4, and 8(4). Quantitative properties are derived from or preserved by linear (ideally, orthogonal) coordinate

transformations. Our treatment of magnification relations in this section will be strictly quantitative in the aforementioned sense, while the next section will employ the qualitative local forms of the families of functions in Arnold's ADE-list.

### Fold and Cusp Magnification Relations

For a locally stable single plane lensing map, the multiple images of a light source near a fold or cusp caustic have distinct configurations locally. Specifically, if the source is near a fold caustic curve, then the multiple images will include a close doublet of images of opposite parity, which then straddle both sides of a critical curve. The image configuration in Figure 11 shows the close doublet for a light source near a fold arc.

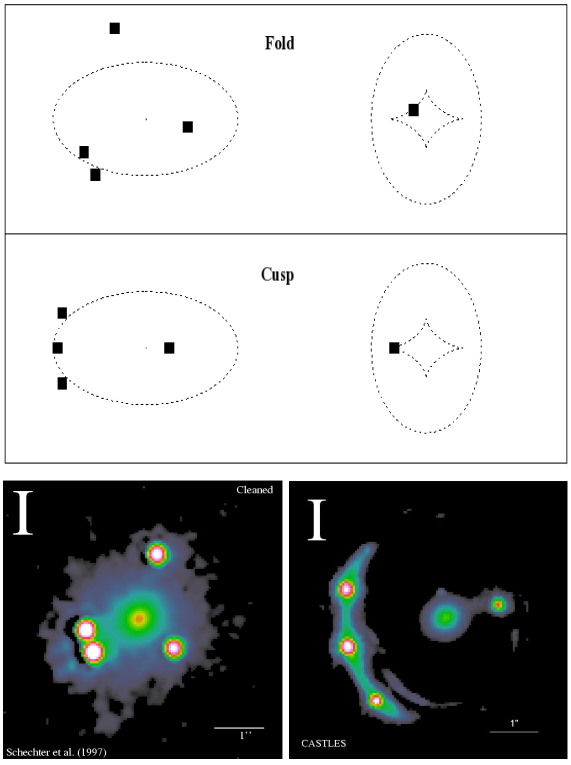


**Figure 11. Top two panels: Predicted multiple image configurations (left) when a source is near a fold caustic arc and cusp caustic point (right). The critical curves are on the left, and the caustics are on the right. A close image doublet and triplet occur for the fold and cusp cases, respectively. The lens model used represents an isothermal ellipsoidal galaxy. Bottom panels: Observed four-image configurations (white discs) of the quasar PG1115 with a fold doublet (bottom left panel) and of the quasar RXJ1131 with a cusp triplet. The observations are in the near-infrared I-band. Credits: Keeton et al. [34] (top panels) and the CASTLES [18] (bottom panels).**

When a light source is near a cusp caustic point and interior to the arcs abutting the cusp, a close triplet of images occurs locally among the lensed images; see Figure 11. The local doublet and triplet image configurations are also predicted from the local form of a locally stable lensing map about a fold caustic point and cusp caustic point, respectively [54, Sec. 9.1]. Observational confirmation of these predictions is given in the bottom panels of Figure 11.

Blandford and Narayan 1986 [16] showed that the close fold image doublet has a total signed magnification that sums to zero:

$$\mu_1 + \mu_2 = 0, \tag{6}$$

where $\mu_1$ and $\mu_2$ are the signed magnifications of the lensed images in the doublet. Since the lensed images in the doublet have opposite parity, if $\mu_1$ and $\mu_2$ have positive and negative parity, respectively, the fold magnification relation can be written as:

$$\frac{|\mu_1|}{|\mu_2|} = 1.$$

A result similar to (6) holds for the close cusp image triplet (Schneider and Weiss 1992 [68] and Zakharov 1995 [76]):

$$\mu_1 + \mu_2 + \mu_3 = 0,$$

where $\mu_1$, $\mu_2$, and $\mu_3$ are signed magnifications of the lensed images in the triplet. These local magnification relations hold independent of the choice of lens model and have been observed.

### Magnification Relations for $D_4^{\pm}$ Caustics

A natural question is whether higher-order caustic magnification relations occur in gravitational lensing. The next theorem due to Aazami and AP 2009 [1] establishes such relations for elliptic and hyperbolic umbilic caustics in lensing.

Let $\eta_{D_4^-}$ and $\eta_{D_4^+}$ denote the respective quantitative local forms of a single-plane lensing map about elliptic umbilic and hyperbolic umbilic caustics; see [66, pp. 200, 201] for their explicit expressions.

**Theorem 13.** [1] *At any noncaustic point of $\eta_{D_4^{\pm}}$ where a light source has four lensed images (the maximum number), the total signed magnification of the light source satisfies:*

$$\mu_1 + \mu_2 + \mu_3 + \mu_4 = 0.$$

Theorem 13 *cannot* be established using the local qualitative forms for caustics in singularity theory. Those forms arise from local diffeomorphisms that distort the lens and light source planes and can transform a lensing map $\eta$ into a map having nothing to do with gravitational lensing. Instead, the quantitative local forms $\eta_{D_4^-}$ and $\eta_{D_4^+}$ of the lensing map in Theorem 13 arise from linear coordinate transformations that preserve the geometric magnification relations under

study. The interested reader may also consult [54, Sec. 9.2] for quantitative local forms of the lensing map about fold and cusp caustics using only orthogonal coordinate transformations.

### Lefschetz Theory and Magnification Relations

We outline the idea behind an alternative proof of Theorem 13 given by Werner 2009 [73] using Lefschetz fixed point theory.

Complexify the polynomial map due to an elliptic umbilic or hyperbolic umbilic singularity to obtain holomorphic maps $f : \mathbb{C}^2 \to \mathbb{C}^2$ such that their fixed points are the four real lensed images of a source at a maximal, noncaustic point (noncaustic locations with the maximum number of lensed images). In this domain, it turns out that the fixed point indices become the signed lensed image magnification, $\det[I - D(f)]^{-1} = \mu$, where $D(f)$ is the matrix of first partial derivatives of $f$ in holomorphic coordinates. If $f$ has no fixed points at infinity, then $f$ can be extended to a holomorphic map $F : \mathbb{CP}^2 \to \mathbb{CP}^2$ for which the holomorphic Lefschetz fixed point formula applies, and we recover $F|_{\mathbb{C}^2} = f$ with the usual decomposition $\mathbb{CP}^2 = \mathbb{C}^2 \cup \mathbb{CP}^1$. Since the holomorphic Lefschetz number for holomorphic maps on complex projective space is unity, we find:

$$\begin{aligned} 1 &= L_{\mathrm{hol}}(F) = \sum_{\mathrm{fix}(F)} \frac{1}{\det[I - D(F)]} \\ &= \sum_{\mathrm{fix}(f)} \frac{1}{\det[I - D(f)]} + \sum_{\mathrm{fix}(F|_{\mathbb{CP}^1})} \frac{1}{\det[I - D(F)]} \\ &= \sum_{i=1}^{4} \mu_i + 1, \end{aligned}$$

where the second equality in the top line is the holomorphic Lefschetz fixed point formula. The result follows; for details see [73] and the review article [57]. Note that the above argument cannot be applied to all stable caustics since there are caustics with fixed points at infinity (e.g., parabolic umbilics).

**Open Problem 7.** Generalize the magnification relations to Lorentzian manifolds.

### Why Are Magnification Relations Important?

The left panel of Figure 12 shows an observed example of multiple images satisfying the fold magnification-relation theorem (6). However, the right panel of Figure 12 has a close fold image doublet that violates the fold magnification relation. What does the violation of a caustic magnification relation signify physically? In 1998 Mao and Schneider [43] interpreted the violation of the cusp magnification relation as the galaxy lens not being smooth on the scale of the angular separation of the images. In other words, there is *substructure* (not detected by our instruments) on the scale of the image separations that affects the image magnifications, thereby causing the violation.

A rigorous and systematic study of the violation of the fold and cusp magnification relations using data was conducted by Keeton, Gaudi, and AP in 2003 [34] and 2005 [35]. For the data sets used in their studies, they showed that five of the twelve fold doublets and three of the four cusp triplets had to arise from galaxy lenses with substructure.

Today, two candidates have emerged for the substructure in the galaxy lenses producing violations of the caustic magnification relations: *dark matter clumps* (Metcalf and Madau 2001 [44] and Chiba 2002 [23]) and *microlensing* by stars with continuous dark matter and shear from infinity (Schechter and Wambsganss 2002 [65]). Both scenarios employ *stochastic gravitational lensing* because the substructure is assumed to be randomly distributed—for instance, the positions of the dark matter clumps or the stars are random vectors.

The planned deep sky surveys [47] for lensing signatures discussed earlier are expected to find examples of high-order caustic magnification relations as well as their violations, which would lead to evidence of substructure in not only galaxies but also clusters of galaxies.

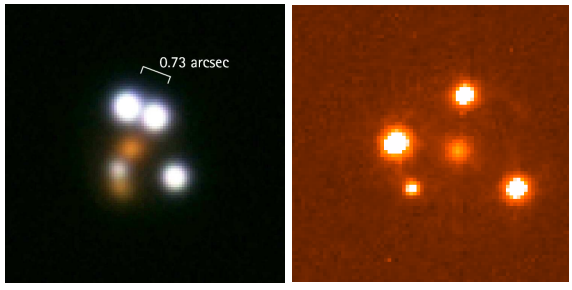


**Figure 12. Left panel: Four lensed images (white blobs) of the lensed quasar HE0230-2130. The fold magnification-relation theorem (i.e., $|\mu_1|/|\mu_2| = 1$) is obeyed by the upper close image doublet because the lensed images are a mere 0.73 arcseconds apart with magnification ratio $|\mu_1|/|\mu_2|$ between 0.9841 and 1.0161. The yellow structure is the location of the deflector galaxy. Right panel: Four lensed images (white blobs) of the lensed quasar SDSS0924+0219, where the yellowish central blob identifies the galaxy lens. The leftmost lensed image pair in the right panel is as close as the doublet in the left panel since the right panel pair has an angular separation of 0.74 arcseconds. However, the right panel pair violates the fold magnification-relation theorem since $|\mu_1|/|\mu_2| = 10$! Credits: Burles (left panel) and Schechter (right panel).**

## The ADE-Magnification Theorem

Aazami and AP 2009 [2] extended their magnification relations in Theorem 13 beyond lensing. They established the result below for the families of functions, not necessarily time-delay families, in Arnold's *ADE* list, which includes caustics with fixed points at infinity.

Let $\mathcal{L}$ be an open subset of $\mathbb{R}^2$ and $S = \mathbb{R}^2$. Consider an $n$-parameter family $F$ of functions $F_{\mathbf{c},\mathbf{s}} : \mathcal{L} \longrightarrow \mathbb{R}$, where $(\mathbf{c},\mathbf{s}) \in \mathbb{R}^{n-2} \times S$. For fixed $(\mathbf{c},\mathbf{s})$, define the *signed magnification* of a critical point $\mathbf{w}_i \in \mathcal{L}$ of $F_{\mathbf{c},\mathbf{s}}$ by:

$$\mathfrak{M}_{\mathbf{c},\mathbf{s}}(\mathbf{w}_i) = \frac{1}{\text{Gauss}\left(\mathbf{w}_i, F_{\mathbf{c},\mathbf{s}}(\mathbf{w}_i)\right)},$$

where the denominator is the Gaussian curvature at $(\mathbf{w}_i, F_{\mathbf{c},\mathbf{s}}(\mathbf{w}_i))$ in the graph of $F_{\mathbf{c},\mathbf{s}}$. Fix $\mathbf{c}_0$ and call $\mathbf{s}' \in S$ a *noncaustic point* if $F_{\mathbf{c}_0,\mathbf{s}'}$ is nondegenerate. Consider the subset $S_0 \subseteq S$ of noncaustic points $\mathbf{s}'$ such that $F_{\mathbf{c}_0,\mathbf{s}'}$ has finitely many critical points, say, $N(\mathbf{s}')$ such points. An element $\mathbf{s}_\times$ of $S_0$ is called a *maximal, noncaustic point* if $N(\mathbf{s}_\times) = \max_{\mathbf{s}' \in S_0} N(\mathbf{s}')$.

**Theorem 14.** [2] *Let $F_{\mathbf{c},\mathbf{s}} : \mathcal{L} \longrightarrow \mathbb{R}$ be any $n$-parameter function in the ADE-family of caustics. Then maximal, noncaustic points exist for each ADE-caustic and for every such point $\mathbf{s}_\times$, the total signed magnification of the critical points $\mathbf{w}_i$ of $F_{\mathbf{c},\mathbf{s}_\times}$ satisfies:*

$$\sum_{i=1}^{N(\mathbf{s}_\times)} \mathfrak{M}_{\mathbf{c},\mathbf{s}_\times}(\mathbf{w}_i) = 0,$$

*where $N(\mathbf{s}_\times) = n+1$ with $n \geq 1$ for $A_{n+1}$ caustics, $N(\mathbf{s}_\times) = n+1$ with $n \geq 3$ for $D_{n+1}$ caustics, $N(\mathbf{s}_\times) = 6, 7, 8$ for $E_6$, $E_7$, $E_8$ caustics, respectively.*

Observe that since magnification is a reciprocal of Gaussian curvature, the magnification relations in Theorem 14 are geometric invariants. Also, note that the theorem singles out the highest-order caustics of each $n$-parameter family.

The proof of Theorem 14 in [2] was algebraic, employing the Euler trace formula [11]. Recently, Aazami, AP, and Rabin 2010 [3] gave an alternative proof using a geometric approach with residues on compact orbifolds. Note that similar to the Lefschetz fixed point approach, direct application of the Euler-Jacobi theorem does not directly yield all the ADE-magnification relations due to nonzero "common roots" at infinity. We end the article with a sketch of the proof in [3].

## Orbifolds and ADE-Magnification Relations

We begin by reviewing the standard residue approach to magnification relations of Dalal and Rabin 2001 [24], which was generalized by Aazami, AP, and Rabin 2010 [3] to orbifolds. For brevity, the proof in [3] will be illustrated using only one singularity from the *ADE*-caustic family. We select the parabolic umbilic caustic $D_5$ since it induces a "lens equation with a root at infinity". To make these ideas precise, we use the fact that the parabolic umbilic arises from the four-parameter family

$$F_{\mathbf{c},\mathbf{s}}(u,v) = u^2 v \pm v^4 + c_3 v^3 + c_2 v^2 - s_2 v - s_2 u.$$

This singularity has a maximal, noncaustic point, which we take to be $\mathbf{s}$, and the maximum number of preimages is five [3]. The parabolic umbilic family $F$ induces a map $\mathbf{f}_\mathbf{c}$ between planes via

$$\mathbf{f}_\mathbf{c}(\mathbf{w}) = \nabla F_{\mathbf{c},\mathbf{s}}(\mathbf{w}) + \mathbf{s},$$

where $\mathbf{w} = (u,v)$. Explicitly: $\nabla F_{\mathbf{c},\mathbf{s}}(\mathbf{w}) = \mathbf{0}$:

$$\begin{aligned} \mathbf{f}_\mathbf{c}(u,v) &= \left(f_\mathbf{c}^{(1)}(u,v)\ ,\ f_\mathbf{c}^{(2)}(u,v)\right) \\ &= \left(2uv\ ,\ u^2 \pm 4v^3 + 3c_3 v^2 + 2c_2 v\right). \end{aligned}$$

Although the $\mathbf{f}_\mathbf{c}$-preimages $\mathbf{w} = (u,v)$ have real coordinates, we shall drop that restriction, allowing for $\mathbf{w} \in \mathbb{C}^2$. Call the critical values of $\mathbf{f}_c$ the *caustic points* of $\mathbf{f}_\mathbf{c}$ since the locus of critical values of $\mathbf{f}_\mathbf{c}$ coincides with the set of $\mathbf{s} \in S$ such that $F_{\mathbf{c},\mathbf{s}}$ has at least one degenerate critical point.

Now, for any noncaustic point $\mathbf{s} = (s_1, s_2)$ of $\mathbf{f}_\mathbf{c}$, consider the following meromorphic two-form on $\mathbb{C}^2$:

$$\omega = \frac{du\, dv}{P_1(u,v) P_2(u,v)},$$

where $P_1(u,v) = f_\mathbf{c}^{(1)}(u,v) - s_1$ and $P_2(u,v) = f_\mathbf{c}^{(2)}(u,v) - s_2$. We are interested only in the poles of $\omega$ that are the common roots of $P_1$ and $P_2$ as they are $\mathbf{f}_\mathbf{c}$-preimages of $\mathbf{s}$. Call such poles the $\mathbf{f}_\mathbf{c}^{-1}(\mathbf{s})$-*poles*. It can be shown that the residue of $\omega$ at $\mathbf{w} \in \mathbf{f}^{-1}(\mathbf{s})$ is precisely the signed magnification $\mathfrak{M}_{\mathbf{c},\mathbf{s}}(\mathbf{w})$, provided $\mathbf{s}$ is not a critical value of $\mathbf{f}_\mathbf{c}$.

Using homogeneous coordinates $[U : V : W]$, where $u = U/W$, $v = V/W$, and $(U,V,W)$ is nonzero, extend $P_1$ and $P_2$, and hence $\mathbf{f}_\mathbf{c}$, to complex projective space $\mathbb{CP}^2$:

(7)

$$\begin{aligned} P_1(U,V,W)_{\text{hom}} &= 2UV - s_1 W^2 \\ P_2(U,V,W)_{\text{hom}} &= U^2 W \pm 4V^3 + 3c_3 V^2 W \\ &\quad + 2c_2 VW2 - s_2 W^3. \end{aligned}$$

Likewise, extend $\omega$ to a 2-form on $\mathbb{CP}^2$ that is homogeneous of degree zero. Its $\mathbf{f}_\mathbf{c}^{-1}(\mathbf{s})$-poles are now the common roots of $P_1$ and $P_2$ in $\mathbb{CP}^2$. Note that $\mathbb{C}^2$ corresponds to $W = 1$ and infinity to $W = 0$.

The global residue theorem [31] states that the sum of the residues of the $\mathbf{f}_\mathbf{c}^{-1}(\mathbf{s})$-poles of $\omega$ on $\mathbb{CP}^2$, which consists of those in $\mathbb{C}^2$ and at infinity, is identically zero. Since the set of poles of $\omega$ in $\mathbb{C}^2$ equals $\mathbf{f}_\mathbf{c}^{-1}(\mathbf{s})$, the sum of their residues is the total signed magnification, $\mathfrak{M}_{\text{tot},\mathbf{c}}(\mathbf{s}) = \sum_{\mathbf{w} \in \mathbf{f}_\mathbf{c}^{-1}(\mathbf{s})} \mathfrak{M}_{\mathbf{c},\mathbf{s}}(\mathbf{w})$. Consequently, the total signed magnification $\mathfrak{M}_{\text{tot},\mathbf{c}}(\mathbf{s})$ is equal to minus the sum of the residues of $\omega$ at infinity.

Recalling that $\mathbf{s}$ is a maximal, noncaustic point of $\mathbf{f_c}$, let us now examine the behavior of the extended parabolic umbilic map $\mathbf{f_c}$ at infinity in $\mathbb{CP}^2$. Setting $W = 0$ in equation (7) yields

$$P_1(U,V,0)_{\text{hom}} = 2UV, \qquad P_2(U,V,0)_{\text{hom}} = \pm 4V^3.$$

These equations have one nonzero common root, which is the $\mathbf{f_c}^{-1}(\mathbf{s})$-pole of $\omega$ at infinity or the $\mathbf{f_c}$-preimage of $\mathbf{s}$ at infinity, namely, the point $[1:0:0]$ in $\mathbb{CP}^2$. As shown in [3], the way around this pole at infinity is to consider an extension to a space other than $\mathbb{CP}^2$, namely, *weighted projective space* $\mathbb{WP}(a_0,a_1,a_2)$, where $a_0, a_1, a_2$ are positive integers denoting particular "weights" of the space. These are examples of compact *orbifolds*.

Orbifolds generalize manifolds. Whereas a manifold locally looks like an open subset of $\mathbb{R}^n$, an orbifold $X$ locally looks like the quotient of an open subset of $\mathbb{R}^n$ by the action of a finite group $G$. The analogues of coordinate charts are known as orbifold charts. Like coordinate charts, two overlapping orbifold charts are required to satisfy a compatibility condition. For our purpose, it is best to distinguish an orbifold $X$ by its *singular points*, which are points $p \in X$ whose stabilizer group $G_p \subset G$ is nontrivial. If an orbifold has no singular points, then it is a smooth manifold. Consult [63, 45, 4] for more on orbifolds.

The most common examples of orbifolds are those which arise as quotients of manifolds by compact Lie groups, and weighted projective space is no exception. For example, the orbifold $\mathbb{WP}(3,2,1)$ is defined by the Lie group action $\mathbb{S}^1 \times \mathbb{S}^5 \longrightarrow \mathbb{S}^5 : (z,(U,V,W)) \longmapsto (z^3U, z^2V, zW)$. So $\mathbb{WP}(3,2,1) = \mathbb{S}^5/\mathbb{S}^1$ under this action, where $\mathbb{S}^1 \subset \mathbb{C}$ and $\mathbb{S}^5 \subset \mathbb{C}^3$. Notice that if the action were $(z,(U,V,W)) \longmapsto (zU, zV, zW)$, then the resulting quotient space would be ordinary complex projective space $\mathbb{CP}^2$. In other words, $\mathbb{WP}(1,1,1) = \mathbb{CP}^2$. Similar to $\mathbb{CP}^2$, the space $\mathbb{WP}(3,2,1)$ has $\mathbb{C}^2$ corresponding to $W = 1$ and infinity to $W = 0$, and $(U,V,W) \neq (0,0,0)$. There are no singular points in the $\mathbb{C}^2$ part of $\mathbb{WP}(3,2,1)$ since the stabilizer condition for such points implies $zW = W$, which forces $z = 1$ and, hence, the stabilizer group to be trivial.

Covering $\mathbb{WP}(3,2,1)$ with homogeneous coordinates $[U:V:W]$, we see that U and V now have weights 3 and 2, respectively, and relate to the coordinates $(u,v) \in \mathbb{C}^2$ in a new way:

$$u = \frac{U}{W^3}, \qquad v = \frac{V}{W^2}.$$

Extending the parabolic umbilic map $\mathbf{f_c}$ to $\mathbb{WP}(3,2,1)$ then yields extensions of $P_1$ and $P_2$ to the following new homogeneous polynomials, respectively:

$$\begin{cases} 2UV - s_1W^5 \\ U^2 \pm 4V^3 + 3c_3V^2W^2 + 2c_2VW^4 - s_2W^6. \end{cases}$$

The two-form $\omega$ then extends to $\mathbb{WP}(3,2,1)$. In $\mathbb{C}^2$, which corresponds to $W = 1$, we recover the same $\mathbf{f_c}$ as in the $\mathbb{CP}^2$ discussion. At infinity or $W = 0$, however, the polynomials become:

$$\begin{cases} 2UV \\ U^2 \pm 4V^3. \end{cases}$$

The only common root is $[0:0:0]$, which is not a point in $\mathbb{WP}(3,2,1)$. In other words, there are no preimages at infinity, hence no $\mathbf{f_c}^{-1}(\mathbf{s})$-poles of $\omega$ at infinity. All the $\mathbf{f_c}^{-1}(\mathbf{s})$-poles then lie in the $\mathbb{C}^2$ part of $\mathbb{WP}(3,2,1)$, where there are no singular points. By the global residue theorem for compact orbifolds, the total signed magnification of the $\mathbf{f_c}$-preimages of the maximal, noncaustic point $\mathbf{s}$ for the parabolic umbilic then satisfies:

$$\mathfrak{M}_{\text{tot},\mathbf{c}}(\mathbf{s}) = \sum_{i=1}^{5} \mathfrak{M}_i = 0.$$

Employing the above procedure with appropriate choices of weighted projective spaces yields magnification relations for *all* the $A, D, E$ singularities; see [3] for details.

### Further Reading

Reference [66] treats the astrophysical aspects of lensing, [54] develops a mathematical theory of lensing for the single and multiplane cases, [57] reviews some mathematical lensing results not covered in this article, and [48] carries out generalizations of lensing to Lorentzian manifolds. The forthcoming book [58] will focus on strong-deflection lensing by black holes and include lensing in Kerr and Fermat geometries.

### Figure Credits

Figure 1, top row: Jerry Schoendorf, MAMS; bottom row, CfA-Arizona Space Telescope LEns Survey (CASTLES) website. Figures 2, 7, 9, 11 courtesy of the author. Figures 3, 4, 6, 10 courtesy of the author and with kind permission of Springer Science and Business Media [see 54]. Figure 5, from [74], H. J. Witt and A. O. Petters, authors. Figure 8, Joachim Wambsganss. Figure 12, left panel: Scott Burles; right panel, Paul Schecter.

## References


[1] A. B. Aazami and A. O. Petters, A universal magnification theorem for higher-order caustic singularities, *J. Math. Phys.* **50** (2009), 032501.

[2] ———, A universal magnification theorem III. Caustics beyond codimension five, *J. Math. Phys.* **51**, 023503 (2010).

[3] A. B. Aazami, A. O. Petters, and J. M. Rabin, Orbifolds, the A, D, E family of caustic singularities, and gravitational lensing, preprint, math-ph arXiv:1004.0516v1 (2010).

[4] A. Adem, J. Leida, and Y. Ruan, *Orbifolds and Stringy Topology*, Cambridge Univ. Press, Cambridge, 2007.

[5] R. ADLER, *The Geometry of Random Fields*, Wiley, London, 1981.
[6] R. ADLER and J. TAYLOR, *Random Fields and Geometry*, Springer, Berlin 2007.
[7] ———, *Applications of Random Fields and Geometry: Foundations and Case Studies*, Springer, Berlin, in press.
[8] V. I. ARNOLD, Normal forms for functions near degenerate critical points, the Weyl groups of $A_k, D_k, E_k$ and Lagrangian singularities, *Func. Anal. Appl.* **6** (1973), 254.
[9] ———, Evolution of singularities of potential flows in collision-free media and the metamorphoses of caustics in three-dimensional space, *J. Sov. Math.* **32** (1986), 229.
[10] ———, *Singularities of Caustics and Wave Fronts*, Kluwer, Dordrecht, 1991.
[11] V. I. ARNOLD, S. M. GUSEIN-ZADE, and A. N. VARCHENKO, *Singularities of Differentiable Maps*, vol. I, Birkhäuser, Boston, 1985.
[12] ———, *Singularities of Differentiable Maps*, vol. II, Birkhäuser, Boston, 1985.
[13] M. V. BERRY, Waves and Thom's theorem, *Adv. Phys.* **25** (1976), 1.
[14] W. BERGWEILER and A. EREMENKO, On the number of solutions of a transcendental equation arising in the theory of gravitational lensing, *Comput. Methods Funct. Theory* **10** (2010), 303.
[15] M. V. BERRY and C. UPSTILL, Catastrophe optics: morphologies of caustics and their diffraction patterns, in *Progress in Optics XVII* (E. Wolf, ed.), North-Holland, Amsterdam, 1980, 257.
[16] R. BLANDFORD and R. NARAYAN, Fermat's principle, caustics, and the classification of gravitational lens images, *Astrophys. J.* **310** (1986), 568.
[17] I. A. BOND, et al., OGLE 2003-BLG-235/MOA 2003-BLG-53: A planetary microlensing event, *Astroph. J. Letters* **606** (2004), L155; see http://www.nd.edu/ bennett/moa53-ogle235/
[18] CASTLES observations lensed quasars and radio sources, http://www.cfa.harvard.edu/glensdata/
[19] J. CALLAHAN, Singularities and Plane Maps II, *Math. Monthly* **84** (1977), 765.
[20] E. CATTANI, A. DICKENSTEIN, and B. STRUMFELS, Computing multidimensional residues, in *Algorithms in Algebraic Geometry and Applications* (L. Gonzalez-Vega and T. Recio, eds.), Birkhäuser, Basel, 1996, 135.
[21] D. CASTRIGIANO and S. HAYES, *Catastrophe Theory*, Addison-Wesley, Reading, MA, 2004.
[22] Y. V. CHEKANOV, Caustics in geometrical optics, *Funct. Anal. Appl.* **20** (1986), 223.
[23] M. CHIBA, Probing dark matter substructure in lens galaxies, *Astrophys. J.* **565** (2002), 17.
[24] N. DALAL and J. M. RABIN, Magnification relations in gravitational lensing via multidimensional residue integrals, *J. Math. Phys.* **42** (2001), 1818.
[25] A. EINSTEIN, Über den Einfluß der Schwerkraft auf die Ausbreitung des Lichtes, *Annalen der Physik* **35** (1911), 898. An English translation is given on p. 99 in: H. LORENTZ, A. EINSTEIN, H. MINKOWSKI, and H. WEYL, *The Principle of Relativity: A Collection of Original Memoirs on the Special and General Theory of Relativity*, Dover, New York, 1952.
[26] ———, Lens-like action of a star by the deviation of light in the gravitational field, *Science* **84** (1936), 506.
[27] Y. ELIASHBERG, On singularities of folding type, *Math. USSR Izvestija* **4** (1970), 1119.
[28] Extrasolar Planets Encyclopedia: http://exoplanet.eu
[29] C. FASSNACHT, C. KEETON, and D. KHAVINSON, Gravitational lensing by elliptical galaxies and the Schwartz function, in *Analysis and Mathematical Physics* (B. Gustafsson and A. Vasilev, eds.), Trends in Mathematics, Birkhäuser, Boston, 2009, 115.
[30] M. GOLUBITSKY and V. GUILLEMIN, *Stable Mappings and Their Singularities*, Springer, Berlin, 1973.
[31] P. GRIFFITHS and J. HARRIS, *Principles of Algebraic Geometry*, Wiley, New York, 1978.
[32] J. GUCKENHEIMER, Caustics and nondegenerate Hamiltonians, *Topology* **13** (1974), 127.
[33] C. R. KEETON, Gravitational lensing with stochastic substructure: Effects of the clump mass function and spatial distribution, preprint, http://xxx.lanl.gov/abs/0908.3001 (2009).
[34] C. KEETON, S. GAUDI, and A. O. PETTERS, Identifying lenses with small-scale structure. I. Cusp lenses, *Astrophys. J.* **598** (2003), 138.
[35] ———, Identifying lenses with small-scale structure. II. Fold lenses, *Astrophys. J.* **635** (2005), 35.
[36] C. R. KEETON and A. O. PETTERS, Formalism for testing theories of gravity using lensing by compact objects. I. Static, spherically symmetric case, *Phys. Rev. D* **72** (2005), 104006.
[37] D. KHAVINSON and R. LUNDBERG, A remark on "Gravitational Lensing and the Maximum Number of Images": 5 radial objects can lens 27 images, preprint (2010). Download from http://shell.cas.usf.edu/~dkhavins/publications.html.
[38] D. KHAVINSON and E. LUNDBERG, Transcendental harmonic mappings and gravitational lensing by isothermal galaxies, *Complex Anal. Oper. Theory*, in press (2010).
[39] D. KHAVINSON and G. NEUMANN, On the number of zeros of certain rational harmonic functions, *Proc. Amer. Math. Soc.* **134** (2006), 1077.
[40] ———, From the fundamental theorem of algebra to astrophysics: A "harmonious" path, *Notices of the AMS* **55**, No. 6 (2008), 666.
[41] L. KUZNIA and E. LUNDBERG, Fixed points of conjugated Blaschke products with applications to gravitational lensing, *Comput. Methods Funct. Theory* **9** (2009), 435.
[42] H. LEVINE, Elimination of cusps, *Topology* **3** (1963), 263.
[43] S. MAO and P. SCHNEIDER, Evidence for substructure in lens galaxies?, *Mon. Not. Roy. Astron. Soc.* **295** (1998), 587.
[44] R. B. METCALF and P. MADAU, Compound gravitational lensing as a probe of dark matter substructure within galaxy halos, *Astrophys. J.* **563** (2001), 9.
[45] I. MOERDIJK and D. A. PRONK, Orbifolds, sheaves, and groupoids, *K-Theory* **12** (1997), 3.
[46] J. F. NYE, *Natural Focusing and Fine Structure of Light*, Institute of Physics Publishing, Bristol, 1999.

[47] G. Orban de Xivry and P. Marshall, An atlas of predicted exotic gravitational lenses, *Mon. Not. Roy. Soc.* **399** (2009), 2.
[48] V. Perlick, *Ray Optics, Fermat's Principle, and Applications to General Relativity*, Springer-Verlag, Berlin, 2000.
[49] A. O. Petters, Singularities in gravitational microlensing, Ph.D. Thesis, MIT, Department of Mathematics, 1991.
[50] ———, Arnold's singularity theory and gravitational lensing, *J. Math. Phys.* **33** (1993), 3555.
[51] ———, Multiplane gravitational lensing. I. Morse theory and image counting, *J. Math. Phys.* **36** (1995), 4263.
[52] ———, Multiplane gravitational lensing. II. Global geometry of caustics, *J. Math. Phys.* **36** (1995), 4276.
[53] ———, Multiplane gravitational lensing. III: Upper bound on number of images, *J. Math. Phys.* **38** (1997), 1605.
[54] A. O. Petters, H. Levine, and J. Wambsganss, *Singularity Theory and Gravitational Lensing*, Birkhäuser, Boston, 2001.
[55] A. O. Petters, B. Rider, and A. M. Teguia, A mathematical theory of stochastic microlensing I. Random time delay functions and lensing maps, *J. Math. Phys.* **50** (2009), 072503.
[56] A. O. Petters, B. Rider, and A. M. Teguia, A mathematical theory of stochastic microlensing II. Random images, shear, and the Kac-Rice formula, *J. Math. Phys.* **50** (2009), 122501.
[57] A. O. Petters and M. C. Werner, Mathematics of gravitational lensing: Multiple imaging and magnification, *Gen. Rel. and Grav.* **42**, 2011 (2010).
[58] A. O. Petters and M. C. Werner, *Gravitational Lensing and Black Holes*, in preparation. Springer, Berlin, 2011.
[59] A. O. Petters and F. W. Wicklin, Caustics of the double-plane two-point-mass gravitational lens with continuous matter and shear, *Mon. Not. R. Astron. Soc.* **277** (1995), 1399.
[60] A. O. Petters and H. Witt, Bounds on the number of cusps due to point mass gravitational lensing, *J. Math. Phys.* **37** (1996), 2920.
[61] J. Renn, T. Sauer, and J. Stachel, The origin of gravitational lensing: A postscipt to Einstein's 1936 *Science* paper, *Science* **275** (1997), 184.
[62] S. H. Rhie, $n$-point gravitational lenses with $5(n-1)$ images, astro-ph/0305166 (2003).
[63] I. Satake, On a generalization of the notion of a manifold, *Proc. Nat. Acad. Sci. USA* **42** (1956), 359.
[64] P. Schneider, The amplification caused by gravitational bending of light, *Astron. Astrophys.* **140** (1984), 119.
[65] P. Schechter and J. Wambsganss, Quasar microlensing at high magnification and the role of dark matter: Enhanced fluctuations and suppressed saddle points, *Astrophys. J.* **580** (2002), 685.
[66] P. Schneider, J. Ehlers, and E. E. Falco, *Gravitational Lenses*, Springer, Berlin, 1992.
[67] P. Schneider and A. Weiss, The two-point mass lens: Detailed investigation of a special asymmetric gravitational lens, *Astron. Astrophys.* **164** (1986), 237.
[68] P. Schneider and A. Weiss, The gravitational lens equation near cusps, *Astron. Astrophys.* **260** (1992), 1.
[69] SLACS: Sloan Lens ACS Survey, where ACS is an acronym for Advanced Camera for Surveys; lensed galaxies (e.g., arcs and rings), `http://www.slacs.org/`
[70] SQLS: lensed quasars in the Sloan Digital Sky Survey data, `http://www-utap.phys.s.u-tokyo.ac.jp/ sdss/ sqls/lens.html`
[71] E. M. Shin and N. W. Evans, The Milky Way Galaxy as a strong gravitational lens, *Mon. Not. Roy. Astron. Soc.* **374** (2007), 1427.
[72] D. Walsh, R. F. Carswell, and R. J. Weymann, 0957+561 A,B: twin quasistellar objects or gravitational lens?, *Nature* **279** (1979), 218.
[73] M. C. Werner, Geometry of universal magnification invariants, *J. Math. Phys.* **50** (2009), 082504.
[74] H. J. Witt and A. O. Petters, Singularities of the one- and two-point mass gravitational lens, *J. Math. Phys.* **4** (1993), 4093.
[75] V. M. Zakalyukin, Reconstruction of fronts and caustics depending on a parameter and versality of mappings, *J. Sov. Math.* **27** (1984), 2713.
[76] A. Zakharov, On the magnification of gravitational lens images near cusps, *Astron. Astrophys.* **293** (1995), 1.